The antiferroelectric crystal structure of the highly ordered complex perovskite $Pb(Yb_{1/2}Nb_{1/2})O_3$

1991 J. Phys.: Condens. Matter 3 2147

(http://iopscience.iop.org/0953-8984/3/13/017)

J. Phys.: Condens. Matter 3 (1991) 2147–2155. Printed in the UK

The antiferroelectric crystal structure of the highly ordered complex perovskite $Pb(Yb_{1/2}Nb_{1/2})O_3$

Jeong Rock Kwon and Woong Kil Choo
Department of Materials Science and Engineering, Korea Advanced Institute of Science and Technology, PO Box 150, Cheongryang, Seoul, Korea

Received 17 October 1990

Abstract. The crystal structure of antiferroelectric $Pb(Yb_{1/2}Nb_{1/2})O_3$ has been characterized. Both x-ray diffraction and transmission electron diffraction show two sets of superlattice reflections originating respectively from the B-site atom ordering and the antiparallel lead-atom displacements which suffer within the orthorhombic a_o–b_o plane along the a_o direction. The room-temperature crystal symmetry is considered to be orthorhombic with space group Pbnm (D_{2h}^{16}) and lattice parameters $a_o = 5.918$ Å, $b_o = 23.453$ Å and $c_o = 8.221$ Å. High-resolution electron microscopy confirms the diffraction results. A structural phase transition from the lower-symmetry phase to the cubic paraelectric phase occurs at about 302 °C on heating.

1. Introduction

A group of complex lead-based perovskite oxides with chemical formula $Pb(B'_xB''_{1-x})O_3$ has been of considerable interest because of the variety of physical properties and the wide range of industrial applications. They have been applied to piezoelectric and pyroelectric devices (Lines and Glass 1977, Burfoot and Taylor 1979).

The physical characteristics of compounds of chemical formula $Pb(B_{1/2}Nb_{1/2})O_3$ ($B \equiv Fe^{3+}$, In^{3+}, Sc^{3+} and Yb^{3+}) belonging to a subgroup of the $Pb(B'_xB''_{1-x})O_3$ group are dependent on the chemical composition and geometrical distribution of the B-site cations in the perovskite lattice. $Pb(Fe_{1/2}Nb_{1/2})O_3$, in which Fe^{3+} and Nb^{5+} ions are randomly distributed on the octahedral sites, is ferroelectric (Lee and Choo 1981). The degree of order among the B-site cations in $Pb(In_{1/2}Nb_{1/2})O_3$ (Groves 1985, Prokopalo *et al* 1982) and $Pb(Sc_{1/2}Nb_{1/2})O_3$ (Stenger and Burggraaf 1980) compounds is reported to be changed by suitable heat treatments. The driving force for order–disorder ability is mainly dependent on the charge and ionic radii differences between the B-site cations. When a high degree of disorder exists among B-site cations, the structural phase transition is usually smeared as a consequence of nanoscale chemical inhomogeneities, and a so-called relaxor phenomenon sets in (Smolenskii 1970, Cross 1987). This relaxor behaviour is characterized by a broad dielectric maximum and frequency-dependent dielectric properties. In contrast, with the increasing degree of B-site order the structural phase transition tends to sharpen.

The compound $Pb(Yb_{1/2}Nb_{1/2})O_3$ (referred to as PYN hereafter) undergoes a paraelectric-to-antiferroelectric phase transition near 310 °C (Tomashpol'skii and

0953-8984/91/132147 + 09 $03.50

Venevtsev 1965) or 302 °C (Isupov and Krainik 1965, Poplavko and Tsykalov 1968). The structure of PYN was first determined by Tomashpol'skii and Venevtsev (1965). They reported that Yb^{3+} and Nb^{5+} ions in PYN alternately occupied the octahedral sites in the perovskite lattice frame. From the x-ray diffraction analysis, its structure was determined to be slightly monoclinic with lattice parameters $a = b = 4.168$ Å, $c = 4.107$ Å and $\gamma = 90° 27'$. They also reported that the x-ray diffraction pattern contained extra lines due to antiparallel cation displacements below the transition temperature. Meanwhile, no superlattice symmetry was determined in their work.

Until now no further study has yet been carried out on the crystal structure of PYN. In this paper we present a detailed investigation of the crystal structure of the antiferroelectric PYN phase by both x-ray diffraction and high-resolution transmission electron microscopy.

2. Experimental method

PYN was prepared by the usual solid state reaction in ceramic form starting from analytical-grade powders of PbO, Yb_2O_3 and Nb_2O_5. The stoichiometric mixtures were mixed in acetone and then calcined at 900 °C for 2 h. Finally, sintering was conducted at 1120 °C for 2 h.

Powders of about 5 μm particle size for x-ray diffraction investigation were prepared by grinding and sieving calcines. They were pressed into a platelet shape. The compact was then attached to the hot-plate, which is housed inside a chamber with a Be window to allow the passage of x-rays. The temperature fluctuation was maintained to within ±0.5 °C. X-ray diffraction experiments were carried out on a two-circle Rigaku diffractometer. Cu Kα radiation was produced by a rotating-anode generator at 40 kV and 120 mA. A curved graphite monochromator was set to reflect the Kα component from the scattered beam. The peaks were scanned continuously in 2θ steps of 0.002° and at a rotating speed of 0.5° min^{-1}.

The ceramic specimen for the electron microscopy study was polished mechanically and thinned further by ion beam milling. All the investigations were performed on a JEOL JEM 2000EX transmission electron microscope with a top-entry goniometer stage at an operating voltage of 200 kV.

3. Results

Figures 1(*a*) and 1(*b*) show x-ray diffraction patterns of a PYN powder sample at 304 °C and room temperature, respectively. Just above the transition as shown in figure 1(*a*), the superlattice reflections (or F reflection) are limited to the sets of diffraction lines that originate from the long-range ordering of Yb^{3+} and Nb^{5+} cations on the octahedral site of the perovskite lattice in addition to the fundamental reflections. The presence of F reflections suggests that the prototypic crystal structure is an ordered perovskite with an effective doubled unit cell ($2a_c \times 2a_c \times 2a_c$) in all crystallographic axis directions of a cubic simple perovskite cell ($a_c \times a_c \times a_c$). Here the subscript c refers to the cubic perovskite subcell.

The room-temperature x-ray diffraction pattern reveals new extra reflections pointing to the formation of a larger superlattice as indicated by full circles in figure 1(*b*). The temperature dependence of these extra reflections is characterized as follows.

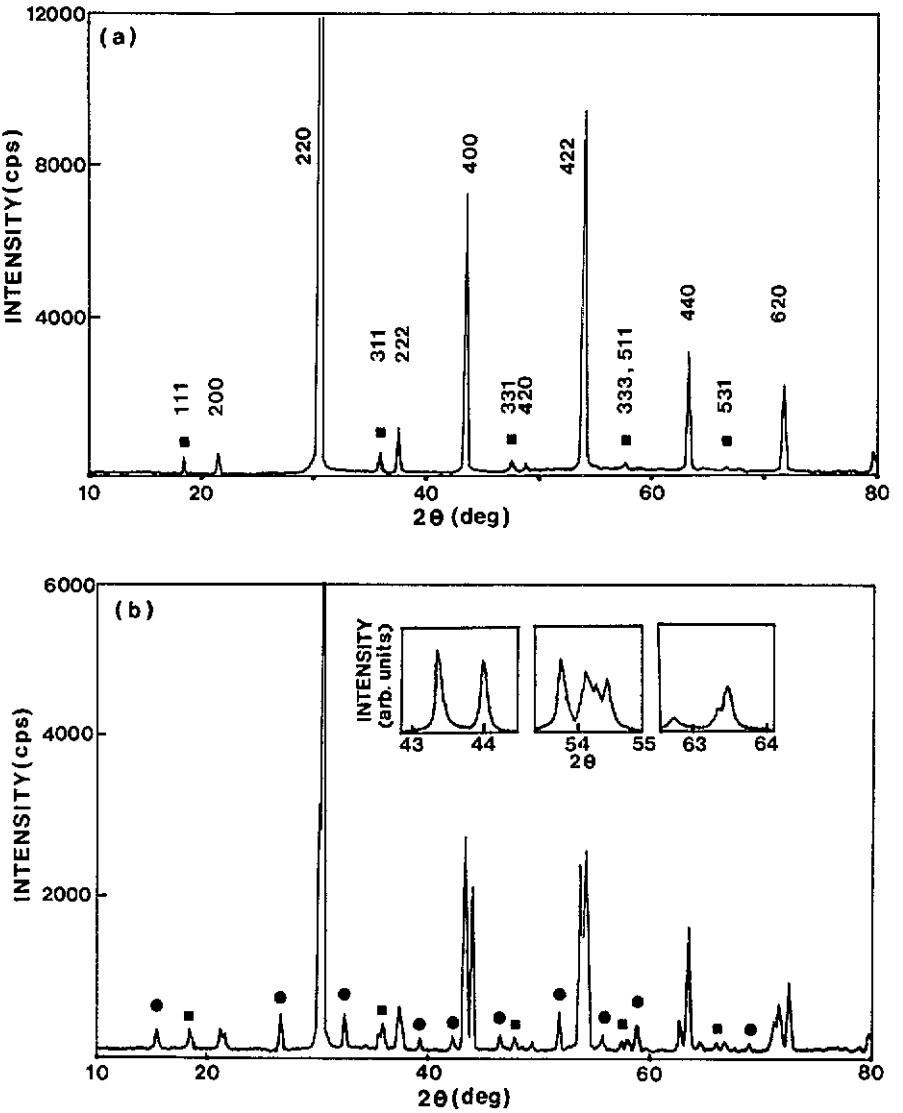

Figure 1. X-ray diffraction patterns of a PYN powder sample at (*a*) 304 °C and (*b*) 20 °C: ■, *F* reflections due to B-site atom ordering; ●, superlattice reflections due to antiparallel cation displacements. The insets in (*b*) clearly show the orthorhombic splittings of selected fundamental lines.

(i) They appear only below the transition temperature of about 302 °C.

(ii) No variation in the line pattern as a function of temperature is observed except the small peak shifts which may be easily attributed to thermal expansion.

(iii) The integrated intensities increase monotonically with decreasing temperature, and a sharp discontinuity in intensities is found near the transition temperature.

This indicates that the cubic-to-orthorhombic transition is first order in nature, a fact which is supported by the sharp dielectric curve and volume discontinuity reported by Tomashpol'skii and Venevtsev (1965).

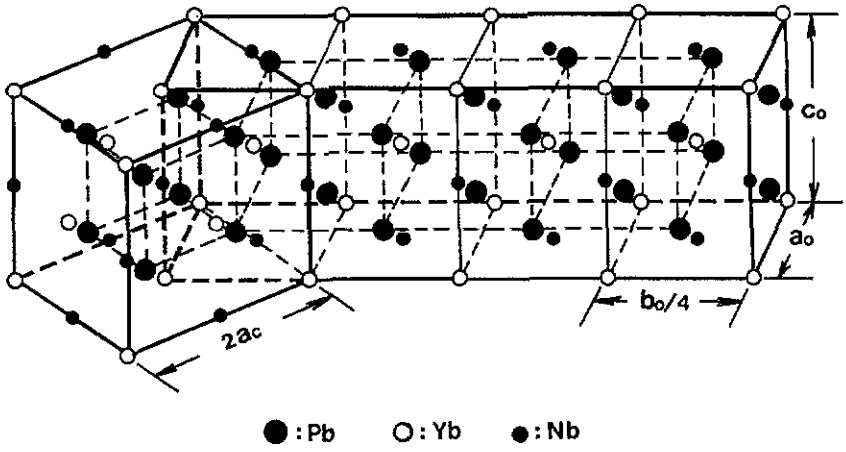

Figure 2. Lattice relationship between high-temperature prototype and low-temperature orthorhombic phases. The Pb^{2+} displacement is not taken into account, and oxygen ion sites are omitted for clarity.

As evidenced from the split in the fundamental lines of the low-temperature phase, as clearly shown in the insets of figure 1(*b*), the lattice distortion is found to be orthorhombic in nature. The unit cell of the room-temperature phase can be constructed from a primitive orthorhombic with lattice parameters $a_o = 5.918$ Å, $b_o = 23.453$ Å and $c_o = 8.221$ Å as shown in figure 2. Here the subscript o refers to the orthorhombic lattice. As a result of the peculiar relation $4a_0 \simeq b_o$ between the two orthorhombic lattice parameters a_o and b_o, both the $(101)_o$ and the $(041)_o$ lines nearly overlap. The lattice relationship between the high-temperature and room-temperature phases is given in figure 2. The orthorhombic basis vectors of the low-temperature phase unit cell have the following relationships with the basis vectors of the prototype phase: $a_o = (a_c + b_c)$, $b_o = 4(-a_c + b_c)$ and $c_o = 2c_c$.

All the new superlattice reflections other than the F reflections are well defined with orthorhombic indices ($h_o \neq 0$, $k_o = 4n \pm 1$ and even l_o). A list of the observed and calculated peak positions together with the approximate intensities is given in table 1. The systematic reflection conditions obtained from x-ray diffraction is summarized as follows: $k_o = 2n$ for $(0kl)_o$; $h_o + l_o = 2n$ or h_o even for $(h0l)_o$; h_o even for $(h00)_o$; l_o even for $(00l)_o$. These conditions may be satisfied by each of four orthorhombic space groups, *Pbnm* (D_{2h}^{16}), *Pbam* (D_{2h}^{9}), *Pba*2 (C_{2v}^{8}) and *Pbn*2_1 (C_{2v}^{9}). It is expected that the latter two, which have no inversion symmetry, are inappropriate for the antiferroelectric crystal structure.

Figure 3(*a*) is the electron diffraction pattern obtained in the $[001]_o$ zone. This pattern is composed of the fundamental spots of the prototype and of the extra superlattice spots in the reciprocal-lattice B* rows. The indexed 140, 200, 080 and 280 spots for instance correspond, respectively, to the 020, 220, $\bar{2}20$ and 040 reflections of the prototype phase. The separation between two nearest fundamental spots in the reciprocal-lattice B* row is again divided into eight equal intervals interspersed by seven superlattice spots. The intensity of these superlattice spots varies in a quasi-manner.

(i) The superlattice spots in the reciprocal lattice $(0k0)_o$ row have only weak intensities, which are not detected in the present x-ray diffraction.

Table 1. Comparison of observed and calculated d-values of x-ray powder diffraction lines, and approximate intensities for orthorhombic PYN. I is the approximate intensity: vw, very weak; w, weak; m, medium; s, strong; vs, very strong.

$(hkl)_o$	d_{obs} (Å)	d_{calc} (Å)	I	$(hkl)_o$	d_{obs} (Å)	d_{calc} (Å)	I
1 1 0[a]	5.722	5.734	w	144	1.843	1.842	vw
1 0 1[b], 0 4 1[b]	4.790	4.786	w	312[a]	1.770	1.842	m
1 4 0	**4.172**	**4.166**	**w**	**342**	**1.703**	**1.703**	
0 0 2	4.112	4.117		1 12 2	1.692	1.693	s
				204	1.686	1.687	
1 1 2[a]	3.341	3.339	m	084	1.682	1.683	
2 0 0	2.962	2.956		234[a]	1.648	1.649	w
080	2.931	2.936	vs				
1 4 2, 1 7 0[a]	2.912	2.925		381[b]	1.601	1.596	vw
2 3 0[a]	2.759	2.766	m	402 254[a]	1.587	1.587	vw
2 4 1[b]	2.523	2.514	m	400	1.480	1.478	
1 8 1[b], 2 5 0[a]	2.510	2.504		0 16 0	1.467	1.465	s
				284	1.464	1.462	
2 0 2	2.399	2.406	m				
0 8 2, 1 9 0[a]	2.388	2.388		314[a], 441[b]	1.414	1.412	vw
2 5 2[a]	2.136	2.137	w	450[a], 404	1.402	1.400	vw
2 8 0	2.084	2.083	s	432[a]	1.362	1.362	vw
0 0 4	2.056	2.054					
				480	1.321	1.320	
1 1 4[a]	1.945	1.940	w	**3 12 2**	**1.316**	**1.316**	s
				146	**1.302**	**1.301**	
2 4 3[b], 3 0 1[b]	1.900	1.896	w				

[a] Superlattice reflection due to antiparallel cation displacements.
[b] Superlattice reflection due to B-site atom ordering.

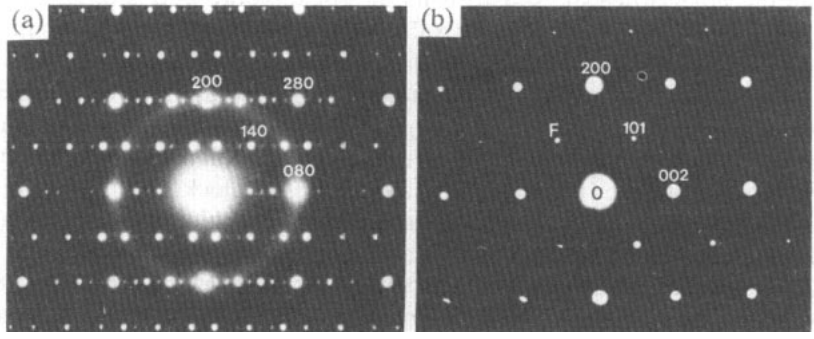

Figure 3. Single-domain electron diffraction patterns of antiferroelectric phase obtained (*a*) in the $[001]_o$ zone and (*b*) in the $[010]_o$ zone.

(ii) The superlattice spots with odd h_o and $k_o = 8n \pm 1$ or even h_o and $k_o = 8n \pm 3$ in $(hk0)_o$ rows have stronger intensities.

These are in agreement with the x-ray diffraction results in which the diffraction lines corresponding to electron diffraction spots such as $(110)_o$ and $(230)_o$ are shown in

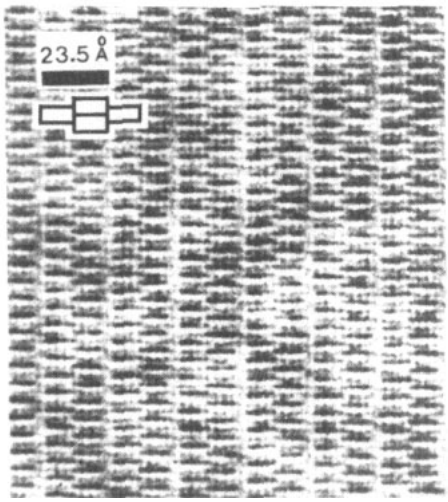

Figure 4. High-resolution image in the $[001]_o$ zone. The inset shows a schematic configuration of the modulated block structure.

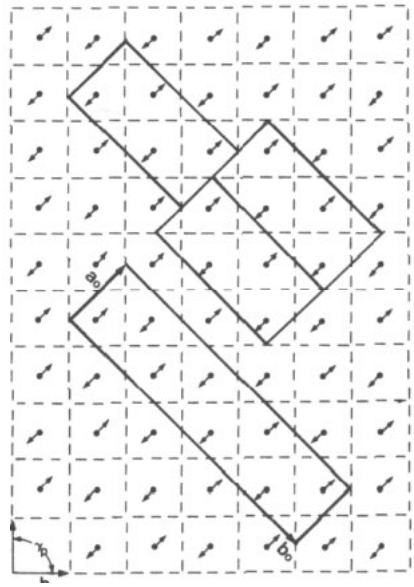

Figure 5. Schematic projection view of the PYN crystal structure along the $[001]_o$ zone axis: – – –, simple perovskite sublattice; —— (upper), block-type arrangement; —— (lower), effective orthorhombic unit cell. The arrows indicate the direction of the Pb^{2+} ion displacements.

figure 1(*b*). The electron diffraction pattern (figure 3(*b*)) obtained in the $[010]_o$ zone is composed of fundamental spots, and the superlattice reflections (or F spots). No resulting superlattice spots apart from the B-cation ordering are observed in this zone in contrast with figure 3(*a*). This result clearly confirms that the extra superlattice spots in figure 3(*a*) arise only along the orthorhombic b_o direction.

In addition to the electron diffraction, high-resolution electron microscopy is of considerable assistance in refining the unit cell. The high-resolution image shown in figure 4, obtained in the $[001]_o$ zone, reveals a modulated structure. The modulated structure is composed periodically of atomic cluster blocks offset by more than half the a_o basis with respect to each other in the a_o direction. A block composed of (2×4) bright dots has a projected repeat length of about 5.86 Å along the a_o direction, i.e. twice the BO_6 octahedra edge length, and a projected repeat length of about 2×5.86 Å in the b_o direction. The true unit-cell length along the b_o direction in the two-dimensional lattice image is twice the block length, i.e. 2×11.72 Å, which translates nicely into the b_o lattice parameter (23.453 Å) obtained from our x-ray measurement.

4. Discussion

The present x-ray diffraction and high-resolution electron microscopy investigations have revealed the existence of a long-period superlattice resulting in orthorhombic symmetry, and the agreement between these two experiments is excellent. A simple

structural description for the antiferroelectric phase based on experimental data will be considered.

In complex perovskites with the allowed occupancy by the two atom species at the B sites, superlattice reflections might generally originate from three components: long-range ordering of B-site cations, antiparallel cation displacements and tilting of the BO_6 octahedra. Displacements of the B-site cations would affect mainly the F reflections. In the x-ray (see figure 1(*b*)) and electron (see figure 3(*a*)) diffractions, no evidence of oxygen atom contribution is detected. This is understandable since the atomic scattering factor of oxygen atoms is small. Hence we see that the extra superlattice reflections mentioned in figures 1(*b*) and 3(*a*) are most likely to originate from the antiparallel displacements of Pb^+ ions. In figures 3(*a*) and (*b*), we note that cation displacements occur only within the orthorhombic a_o–b_o planes, which is consistent with the x-ray results that displacement superlattice reflections with odd l_o are not observed. The x-ray diffraction results in figure 1 alone cannot distinguish between two space groups, *Pbnm* and *Pbam*, since both $(101)_o$ and $(041)_o$ peaks are nearly superposed owing to the peculiar relation $4a_o \simeq b_o$. However, the presence of $(101)_o$ and $(301)_o$ spots in the $[010]_o$ zone in figure 3(*b*) confirm the space group symmetry *Pbnm*. Concerning the Pb, Yb and Nb arrangements, the most probable space group symmetry derived from both x-ray and electron diffraction is *Pbnm* (D_{2h}^{16}). From this space group consideration, we interpret that the main displacements of Pb^{2+} cations occur within the $(001)_o$ plane along the orthorhombic a_o direction.

Figure 5 shows the $[001]_o$ projection view of the schematic antiferroelectric atomic arrangement in PYN, which is found to be consistent with our experimental evidence. The periodicity along the c_o axis is the same as that of the prototype phase. In the figure the arrows show the direction of Pb^{2+} ion displacements, and the B-site Yb^{3+} and Nb^{5+} cations are located alternately at the corners of the simple perovskite unit cell drawn as broken lines. Here only the Pb^{2+} ion displacement is taken into consideration since the BO_6 octahedral tilting contributions to scattering are negligible in comparison with that of the Pb cations, as referred to above. The intensity profile of x-ray diffraction lines has been simulated with different sets of displacement values to find the optimum fit to the experimental x-ray diffraction pattern. With $\delta\,(=\Delta a_o/a_o) = 0.041$, the best fit was obtained. We thus find that the Pb^{2+} displacement Δa_o is about 0.24 Å along the a_o direction. The block structure of three small rectangles delineated by full lines is clearly related to the high-resolution image in the $[001]_o$ zone as shown in figure 4. The lower rectangle shows the effective orthorhombic unit cell. As discussed so far, the diffraction characteristics as well as the lattice image may be best explained by the Pb^{2+} displacement along the a_o axis with long periodicity in the b_o direction. In the appendix, the structure factor F_{hkl} of the orthorhombic unit cell which is necessary to find the fractional displacement δ is derived.

Lead zirconate ($PbZrO_3$) is the well known and thus far the best studied antiferrodistortive antiferroelectric (Sawaguchi *et al* 1951, Jona *et al* 1957, Fujishita *et al* 1982), where the crystal structure is characterized by the antiparallel Pb^{2+} displacement. Its crystal symmetry is similar to that of PYN with slight difference. The commensurate lattice modulation and unique lattice parameter relation $b_o \simeq 2a_o$ for $PbZrO_3$ between orthorhombic a_o and b_o axes are different from $b_o \simeq 4a_o$ for PYN. Most probably, the structural difference between these two compounds may be ascribed to the B-site ordering in PYN.

The first-order approximation for the PYN structure factor as derived in appendix can fully account for the x-ray lines ascribed to the B-site ordering and transverse Pb^{2+}

ion displacement, but not for the electron superlattice spots aligned in the $[010]_o$ direction. The presence of the very weak superlattice spots aligned in figure 3(*a*) may be due to a small shift of the Pb^{2+} ion along the orthorhombic b_o direction in addition to the a_o direction. Since neither x-ray diffraction nor electron transmission microscopy is sensitive to the oxygen atom scattering, a further structural investigation is deemed necessary to find the oxygen contribution to the physical properties at this point.

5. Conclusions

On the basis of both x-ray and electron diffraction observations, we have shown that the antiferroelectric $Pb(Yb_{1/2}Nb_{1/2})O_3$ has a long-period structure derived from antiparallel dipole ordering between the neighbouring perovskite sublattices. Also, high-resolution image information supports our structural model based on the antiparallel Pb^{2+} displacement, which renders a strong argument for antiferroelectric nature of PYN.

The lattice modulation associated with the antiparallel Pb^{2+} displacement arises only within the orthorhombic a_o–b_o plane. The room-temperature crystal symmetry is determined to be orthorhombic with space group *Pbnm* (D_{2h}^{16}) and lattice parameters $a_o = 5.918$ Å, $b_o = 23.453$ Å and $c_o = 8.221$ Å. On heating, PYN transforms to a cubic paraelectric phase at about 302 °C.

Acknowledgments

The authors would like to thank S S Park who wrote the computer program for our crystal structure analysis. One of the authors (WKC) is grateful to the Korea Science and Engineering Foundation who provided partial funding for this study.

Appendix

Before analysing the experimental x-ray diffraction pattern of PYN, it is necessary to calculate the structure factor of the orthorhombic unit cell shown in figure 5. The cation sites based the orthorhombic system are hence given as follows: Pb^{2+} at $(\frac{1}{4}+\delta\ \frac{1}{16}\ \frac{1}{4})$, $(\frac{3}{4}-\delta\ \frac{3}{16}\ \frac{1}{4})$, $(\frac{1}{4}+\delta\ \frac{5}{16}\ \frac{1}{4})$, $(\frac{3}{4}-\delta\ \frac{7}{16}\ \frac{1}{4})$, $(\frac{1}{4}-\delta\ \frac{9}{16}\ \frac{1}{4})$, $(\frac{3}{4}+\delta\ \frac{11}{16}\ \frac{1}{4})$, $(\frac{1}{4}-\delta\ \frac{13}{16}\ \frac{1}{4})$, $(\frac{3}{4}+\delta\ \frac{15}{16}\ \frac{1}{4})$, $(\frac{1}{4}+\delta\ \frac{1}{16}\ \frac{3}{4})$, $(\frac{3}{4}-\delta\ \frac{3}{16}\ \frac{3}{4})$, $(\frac{1}{4}+\delta\ \frac{5}{16}\ \frac{3}{4})$, $(\frac{3}{4}-\delta\ \frac{7}{16}\ \frac{3}{4})$, $(\frac{1}{4}-\delta\ \frac{9}{16}\ \frac{3}{4})$, $(\frac{3}{4}+\delta\ \frac{11}{16}\ \frac{3}{4})$, $(\frac{1}{4}-\delta\ \frac{13}{16}\ \frac{3}{4})$, $(\frac{3}{4}+\delta\ \frac{15}{16}\ \frac{3}{4})$; Yb^{3+} at $(\frac{3}{4}\ \frac{1}{16}\ 0)$, $(\frac{3}{4}\ \frac{5}{16}\ 0)$, $(\frac{3}{4}\ \frac{9}{16}\ 0)$, $(\frac{3}{4}\ \frac{13}{16}\ 0)$, $(\frac{1}{4}\ \frac{3}{16}\ \frac{1}{2})$, $(\frac{1}{4}\ \frac{7}{16}\ \frac{1}{2})$, $(\frac{1}{4}\ \frac{11}{16}\ \frac{1}{2})$, $(\frac{1}{4}\ \frac{15}{16}\ \frac{1}{2})$; Nb^{5+} at $(\frac{1}{4}\ \frac{3}{16}\ 0)$, $(\frac{1}{4}\ \frac{7}{16}\ 0)$, $(\frac{1}{4}\ \frac{11}{16}\ 0)$, $(\frac{1}{4}\ \frac{15}{16}\ 0)$, $(\frac{3}{4}\ \frac{1}{16}\ \frac{1}{2})$, $(\frac{3}{4}\ \frac{5}{16}\ \frac{1}{2})$, $(\frac{3}{4}\ \frac{9}{16}\ \frac{1}{2})$, $(\frac{3}{4}\ \frac{13}{16}\ \frac{1}{2})$; δ refers to the fractional displacement ($\delta = \Delta a_o/a_o$) of lead cation. Here, the oxygen contribution to the intensity of the diffracted lines is neglected because of the small oxygen scattering factor in comparison with those of the cations. Assuming only the transverse Pb^{2+} ion displacement, we can write the structure factor F_{hkl} to the first-order approximation as follows:

$$\begin{aligned}F_{hkl} = f_{Pb}[1+(-1)^l][1+(-1)^{k/2}]\exp[2\pi i(h/4+k/16+l/4)]\\ \times\{[\exp(2\pi\delta hi)+(-1)^k\exp(-2\pi\delta hi)]+[\exp(-2\pi\delta hi)\\ +(-1)^k\exp(2\pi\delta hi)]\exp[2\pi i(h/2+k/8)]\}+[1+(-1)^k][1+(-1)^{k/2}]\\ \times\exp[-2\pi i(h/4+k/16)]\{[f_{Nb}+(-1)^l f_{Yb}]\\ \times\exp(\pi ki/4)+[f_{Yb}+(-1)^l f_{Nb}]\exp(\pi hi)\}\end{aligned}$$

where f_{Pb}, f_{Nb} and f_{Yb} refer to the ionic scattering factors of Pb^{2+}, Nb^{5+} and Yb^{3+} respectively, and (hkl) are the plane indices of the orthorhombic cell. The omission of oxygen scattering is justified because in the x-ray diffraction no oxygen contribution is detected. An extinction condition may be first derived as follows.

(i) When $k = 4n \pm 2$, $F_{hkl} = 0$.

The fundamental diffraction lines satisfy the following selection rules.

(ii) When $k = 4n$ and even l, $F_{hkl} \neq 0$.
(iii) When $k = 4n \pm 1$ (or $4n \pm 3$) and odd l, $F_{hkl} \neq 0$.

With the above selection rules, the structure factor contribution from the Yb^{3+} and Nb^{5+} ordering may be written separately as follows.

(iv) When $h \neq 4k$, $k = 4n$ and odd l, $F_{hkl} = 4(f_{Yb} - f_{Nb}) \exp[2\pi i(h/4 + k/16)] \times [\exp(\pi hi)] - \exp(\pi ki/4)]$.

After the fundamental and order-related superlattice reflections are taken, the structure factor contribution from the Pb^{2+} displacement may be written as follows.

(v) When $k = 4n \pm 1$ (or $4n \pm 3$) and even l, $|F_{hkl}| = 8f_{Pb}|\sin(2\pi h\delta)|\,|\{\exp[2\pi i(h/4 + k/16 + l/4)]\,(1 - \exp[2\pi i(h/2 + k/8)])\}|$.

The last condition shows that the intensity of superlattice reflections such as (110) and (230), etc, depends on the Pb^{2+} displacement δ as well as on the plane indices. Using the general structure factor formula, x-ray diffraction powder patterns have been simulated on an IBM AT compatible to fit the experimental data with the δ-value as a variant. The nominal δ-value was chosen when the computer simulation fits the experimental data optimally.

References

Burfoot J C and Taylor G W 1979 *Polar Dielectrics and Their Applications* (Macmillan: London) p 559
Cross L E 1987 *Ferroelectrics* **76** 241
Fujishita H, Shiozaki Y, Achiwa N and Sawaguchi E 1982 *J. Phys. Soc. Japan* **51** 3583
Groves P 1985 *J. Phys. C: Solid State Phys.* **18** L1073
Isupov V A and Krainik N N 1965 *Sov. Phys.–Solid State* **6** 2975
Jona F, Shirane G, Mazzi F and Pepinsky R 1957 *Phys. Rev.* **15** 849
Lee M H and Choo W K 1981 *J. Appl. Phys.* **52** 5767
Lines M E and Glass M A 1977 *Principles and Applications of Ferroelectrics and Related Materials* (Oxford: Clarendon) p 296
Poplavko Yu M and Tsykalov 1968 *Sov. Phys.–Solid State* **9** 2600
Prokopalo O I, Raevskii J P, Malitskaya M A, Popov Y M, Bokov A A and Smotrakkov V G 1982 *Ferroelectrics* **45** 89
Sawaguchi E, Maniwa H and Hoshino S 1951 *Phys. Rev.* **83** 1078
Smolenskii G A 1970 *J. Phys. Soc. Japan, Suppl.* **28** 26
Stenger C G F and Burggraaf A J 1980 *Phys. Status Solidi* a **61** 653
Tomashpol'skii Y Y and Venevtsev Y N 1965 *Sov. Phys.–Solid State* **6** 2388